COMPDYN 2013
4th ECCOMAS Thematic Conference on
Computational Methods in Structural Dynamics and Earthquake Engineering
M. Papadrakakis, V. Papadopoulos, V. Plevris (eds.)
Kos Island, Greece, 12–14 June 2013

STATISTICAL EVALUATION OF THE SEISMIC SERVICEABILITY OF A BULLET TRAIN ALONG THE DEAD SEA FAULT

Shun Uchida[1] **and Assaf Klar**[2]

[1]Technion - Israel Institute of Technology
Technion City, Haifa 32000, Israel
e-mail: shun@icoeng.com

[2] Technion - Israel Institute of Technology
Technion City, Haifa 32000, Israel
e-mail: klar@technion.ac.il

Keywords: probabilistic seismic hazard analysis, nonlinear soil behavior, CAV, stochastic soil properties, differential displacement, Dead sea fault

Abstract. *The bullet train from Be'er-Sheva to Eilat in Israel is planned to be built in great vicinity to the Dead Sea Fault (DSF) and therefore susceptible to different seismic risks. Bullet trains are especially vulnerable to differential deformations and one of the engineering tasks associated with the train design is to evaluate the expected serviceability level with time.*

The paper presents statistical analyses conducted for the prediction of the anticipated deformation of the railway caused by multiple and single earthquake events as function of the exposure period. The analyses incorporate both a probabilistic seismic hazard analysis (PSHA) and statistical disaggregation to select controlling events, using local seismicity data.

The highlight of the analyses is its comprehensive approach to include four main features, from viewpoints of geotechnical engineering and earthquake engineering. Firstly, the soil constitutive model considers the effects of nonlinearity and plastic compaction due to cyclic loading. Plastic deformations during earthquakes are widely known phenomena and thus important to be taken into account for accurate deformation prediction. Secondly, the soil properties are distributed heterogeneously so that differential deformations can be evaluated, which are likely to occur in natural sediments. Thirdly, using an attenuation model, a potential cumulative absolute velocity (CAV) is evaluated at different return period based on Israeli local seismic zones and levels. Using statistical disaggregation, well representative earthquakes are selected and used for geomechanical analyses in order to predict deformation patterns. Forth, based on the results of 81 cases investigated, the fragility curves for the serviceability of the train are plotted. The resulting curves can be used as guideline to build the railway track for given exposure period of the structure and deformation tolerance.

1 INTRODUCTION

The high-speed train from Be'er-Sheva to Eilat in Israel is planned to be built in great vicinity to the Dead Sea Fault (DSF) and therefore susceptible to different seismic risks. High-speed trains are especially vulnerable to differential deformations and one of the engineering tasks associated with the railway design is to evaluate the expected serviceability level with time.

This paper presents statistical analysis for the prediction of the differential deformation of the railway track caused by single and multiple earthquake events. The highlight of the analysis is its comprehensive approach to incorporate advanced features from viewpoints of both earthquake engineering and geotechnical engineering. The former is the use of a probabilistic seismic hazard analysis (PSHA) [1], which integrates all possible earthquake ground motions (i.e. magnitudes, locations, and ground conditions). The latter is that the analysis also incorporates nonlinear soil behavior and heterogeneous soil properties in order to better represent true soil behavior.

2 MODELLING PROCEDURE

2.1 Model geometry

Fig. 1 shows the considered model geometry with the boundary conditions. In the analysis, it is assumed that a railway track is placed on top of an embankment, which has height of 10 meters, width of 15 meters and a sides slope of 25 degrees. Similar analysis should be repeated for other dimensions. Earthquake velocities are applied at the bottom of the base sediment and they are calibrated from the outcrop accelerations of several real earthquakes (discussed later). The lower boundary constitutes a transmitting boundary allowing any reflected waves to propagate downwards. The side boundaries are set such that they form periodic boundaries. The location of the considered site is in the middle range of the route of rail, at the middle of the Arava as shown later as the red circle in Fig. 5.

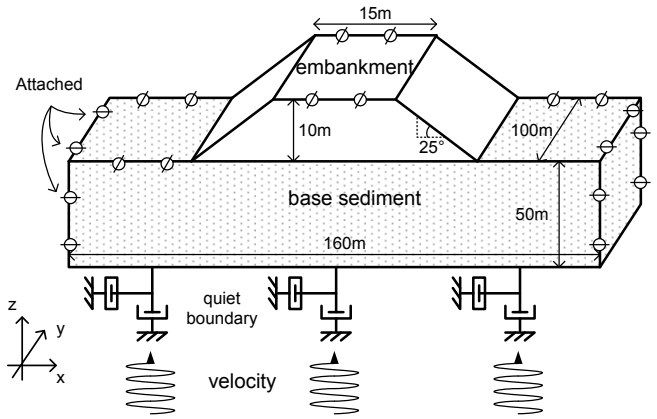

Figure 1: Model geometry and boundary conditions

2.2 Soil model

During earthquakes, the soil is subjected to cyclic loading. It is widely known that cyclic loading induces volumetric and deviatoric plastic deformation. Fig. 2 shows an idealized stress-

strain relation of a drained soil under cyclic loading. If the soil is a linear elastic material (i.e. no plastic deformation), the soil stresses and strains return to the original state at the end of loading cycle. However, in reality, the soil comprises grains which are rearranged due to shearing. The rearrangement of particles leads to both nonlinear plastic behavior in the deviatoric and volumetric spaces.

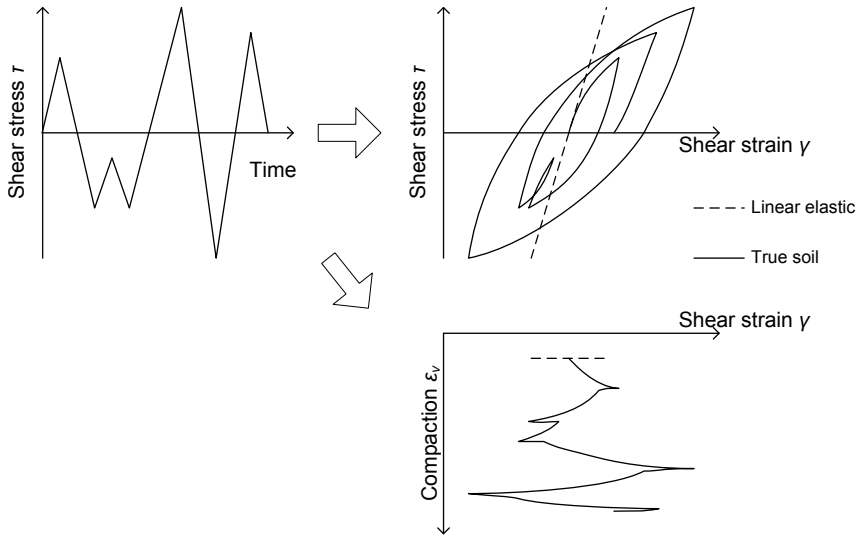

Figure 2: Idealised stress-strain and volumetric behaviour under cyclic loading

This plastic behavior is controlled by a nonlinear backbone curve that can be define using the degradation model suggested by [2],which is shown in Fig. 3a and given by:

$$\frac{G}{G_{max}} = \frac{1.014}{1 + \exp[-(\log\gamma - 1.249)/(-0.4792)]} \tag{1}$$

where G_{max} is the maximum shear stiffness (discussed in the next section) and γ is the shear strain. For the plastic compaction, the model by [3] is used, which is shown in Fig. 3b and given by:

$$\frac{\Delta\epsilon_v^p}{\gamma} = C_1 \exp\left[-\frac{0.4}{C_1}\frac{\epsilon_v^p}{\gamma}\right] \tag{2}$$

where ϵ_v^p is the plastic volumetric strain and C_1 is the soil parameter, which is related to density of soil (discussed in the next section).

It should be noted that when the soil is saturated with water, the reduction of pore space due to shear loading induces excess pore pressure and thus the effective stresses decrease (i.e. liquefaction if the effective stresses become zero). The reduction of effective stresses further decreases the soil stiffness. Thus, additional deformation is expected if the soil is saturated. While the current analysis does not consider this effect, the constructed model would be able to evaluate such conditions if required.

2.3 Stochastic soil properties

No differential deformation will develop (even longitudinally along a section of the railway track) when the soil is homogeneous in horizontal direction. This implies that, unless true

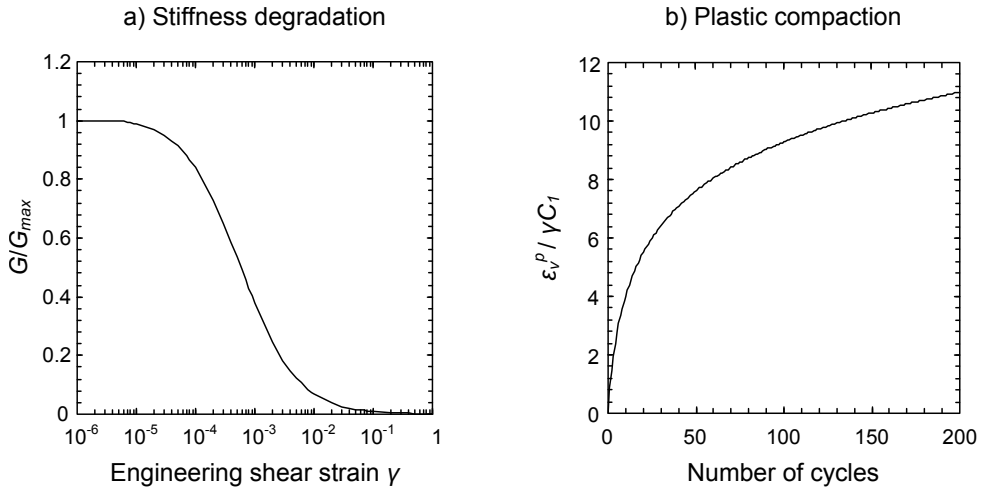

Figure 3: Models used for representation of grain rearrangement

variation of soil properties are considered, even a three-dimensional model will predict zero differential deformation (for the considered geometry). Natural sediments are heterogeneous and thus likely to cause differential deformation which may hinder serviceability of the railway track. The current analysis attempts to capture these important characteristics in a realistic manner by the following.

The current analysis adopts the normalized blow counts of Standard Penetration Test (SPT), $(N_1)_{60}$ ($= N\sqrt{p_a/\sigma'_z}$ [2], where p_a is atmospheric pressure), as an input and assumes that the values follow a normal Gaussian distribution. For the base soil, the distribution has the mean $(N_1)_{60}$ value of 20 ($\approx$ relative density of 70 %) with a coefficient of variation of 26 % (suggested by [4]). For the embankment, assuming thorough compaction is conducted, the mean $(N_1)_{60}$ value is set to be 35 ($\approx$ relative density of 89 %) with a coefficient of variation of 10 %.

In addition, in order to better represent natural soil properties, the distributed values are also spatially auto-correlated, that is, the values are correlated in relatively close locational positions (i.e. auto-correlation distance), rather than being completely random. A large auto-correlation distance implies that the soil property is highly correlated over a large spatial extent, resulting in a smooth variation within the soil profile. In this study, auto-correlation distance is set to be 10-20 m (based on work by [5]). Fig. 4 presents the distributions of the normalized SPT value in studied three cases, which are hereafter referred to as "Soil 1", "Soil 2" and "Soil 3".

The spatially distributed and auto-correlated $(N_1)_{60}$ are used to obtain the maximum shear stiffness G_{max} by [6]:

$$G_{max} = 21.7 \cdot p_a \cdot 20(N_1)_{60}^{1/3} \left(\frac{p'}{p_a}\right)^{0.5} \tag{3}$$

where p' is the mean effective stress. The plastic compaction model parameter C_1 is also obtained from $(N_1)_{60}$ by [3]:

$$C_1 = 8.7(N_1)_{60}^{-1.25} \tag{4}$$

A larger $(N_1)_{60}$ indicates that the soil is stiff and thus the maximum shear stiffness becomes large. As stiffer soil tends to induce less plastic strain, C_1 becomes smaller with increasing $(N_1)_{60}$. These values are used for the nonlinear soil model as described in Fig. 3.

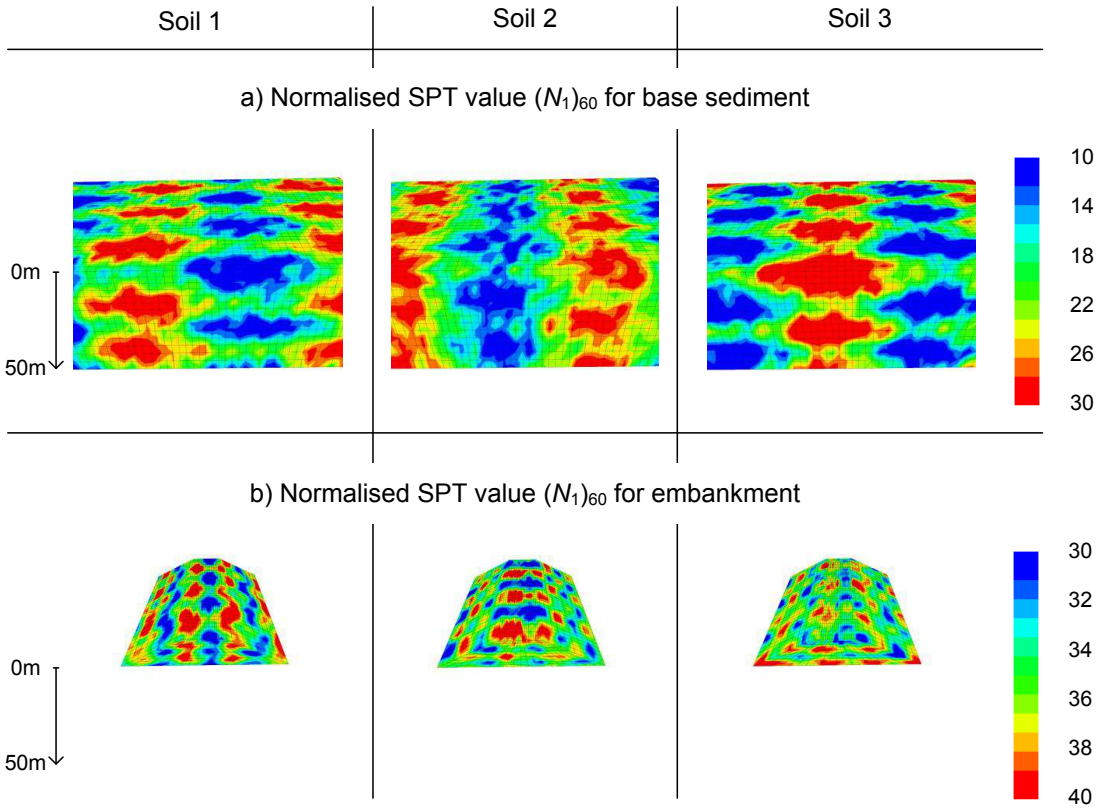

Figure 4: Distributions of normalised SPT value

3 PROCEDURE OF SELECTING EARTHQUAKES FOR TIME-DOMAIN ANALYSIS

This section describes the procedure of selecting input earthquake acceleration time histories for the analysis. This study takes an approach of probabilistic seismic hazard analysis incorporating:

- An attenuation model to evaluate cumulative absolute velocity (CAV) at a given return period based on the Israeli seismogenic zone;
- Disaggregation (or deaggregation) model to determine the dominant contributing factors (e.g. magnitude or location) to the estimated CAV;
- Scaling of real earthquake acceleration time history.

A Probabilistic Seismic Hazard Analysis (PSHA) is a probability-based framework capable of quantifying various ground-motion values (e.g. peak ground acceleration) at a considered site. It is known that ground-motion values vary with many uncertain factors such as location of the earthquake, fault type, variability of ground motion intensity, characteristics of ground and probability of occurrence of earthquake itself. Rather than ignoring the uncertainties present in earthquake-related problem, PSHA incorporates them into the calculation of potential ground motion intensities.

3.1 Potential cumulative absolute velocity based on its return period

Cumulative absolute velocity (CAV), defined as the integral of the absolute acceleration time series, has been used as an index to indicate the possible onset of structural damage and liquefaction of saturated soils. Although named the cumulative absolute velocity, CAV is not directly related to the ground motion velocity, rather, it originates from the fact that the integral over acceleration can be rewritten as summation of incremental (i.e., peak-to-valley and valley-to-peak) velocities. Thus, the value CAV is an indicator of cyclic loading. Since its introduction in 1988, a number of studies have shown that CAV is better predictor (also smaller standard deviation) than other energy related intensity measures such as Peak Ground Acceleration (PGA) of potential damage of soil and structures, which are prone to cyclic loading or fatigue failure [7, 8, 9, 10].

To obtain the exceedance value of CAV through PSHA analysis, one must consider all possible earthquake events (magnitude and distances) that may affect the site. In this work, the Israeli Catalogue of seismogenic zones by [11] is adopted. The solution, based on event occurrence following the Gutenberg-Richter with a limit on the maximum magnitude, may be obtained numerically by the following integral:

$$\lambda_{z^*}(x_0, y_0, z^*) = \sum_{i=1}^{NS} \sum_{k=NXS_i}^{NXE_i} \sum_{l=NYS_i}^{NYE_i} \sum_{j=1}^{NMW} \alpha_i P[z^*|m_j, r_{i,k,l}] f_{Mi,j} A_{i,k,l} \Delta m_i \tag{5}$$

$$m_j = M_{min,i} + (j - 0.5)\Delta m_i \tag{6}$$

$$r_{i,k,l} = \sqrt{(x_0 - (k - 0.5)\Delta x)^2 + (y_0 - (l - 0.5)\Delta y)^2} \tag{7}$$

$$f_{Mi,j} = \frac{\beta_i \exp[-\beta_i (j - 0.5)\Delta m_i]}{1 - \exp[-\beta_i (M_{max,i} - M_{min,i})]} \tag{8}$$

$$A_{i,k,l} = \frac{PIZ(i, (k - 0.5)\Delta x, (l - 0.5)\Delta y)}{NR_i} \tag{9}$$

$$\Delta m_i = \frac{M_{max,i} - M_{min,i}}{NMW} \tag{10}$$

where λ_{z^*} is the return period of the ground motion parameter of question z^* (CAV and PGA in this work), (x_0,y_0) are the coordinates for which this value z^* is evaluated, α_i, β_i, $M_{min,i}$, and $M_{max,i}$ are parameters of the Guttenberg-Richter (bounded by upper magnitude) model for the seismicity of the seismogenic zones of Israel (shown in Fig. 5 and given in Table 1), NS is the total number of seismogenic zones, NXS_i, NYS_i, NXE_i and NYE_i are the boundaries of indexes k and l for each seismogenic zone to form a rectangular in which the seismogenic zone is encompassed, NMW is the division of magnitude in the integration, $P[z^*|m_j, r_{i,k,l}]$ is the probability that the ground motion parameter at point (x_0, y_0) due to an event with magnitude m_j at distance $r_{i,k,l}$ will be larger than z^*, NR_i is the number rectangular element of size Δx times Δy found in seismogenic zone i and PIZ is a special function which gives one if the currently considered source (which is integrated for the all the area) is found in seismogenic zone i and zero otherwise. Note that in the solution we search for z^* that will give the required return period $R = 1/\lambda_{z^*}$.

A design return period R is the average interval of time between events leading to an equal or greater associated ground motion parameter. It may be used to define the exceedance probability P_e (i.e. probability that at least one event would occur) for a given exposure period t (or vice versa), using Poisson's model as:

$$P_e = 1 - \exp[-t/R] \tag{11}$$

Incorporating Campbell and Bozorgnia attenuation model [12] with its defined standard deviation into Eq. 5 (as part of $P[z^*|m_j, r_{i,k,l}]$) gives a solution for defining the CAV at the considered site in the Arava. It should be noted that the ground motion component used to define CAV in this study is the geometric mean of the two recorded horizontal components (often noted as $\mathrm{CAV_{gm}}$).

Fig. 6 shows the estimated CAV (and PGA for a comparison) with increasing return period at the considered site in the Arava. For example, at return period of 160 years, the expected CAV is 3.46 m/s. This implies that, at the Arava site, a chance of which CAV caused by earthquakes would exceed 3.46 m/s, at least once in 100 years, is 46 % (or 27 % in 50 years). The values given in Fig. 6 are calculated for a site with shear wave velocity v_s=180 m/s (classified as soil Type D by the Israeli standard, following ASCE-7-05 classification).

3.2 Disaggregation for a given CAV

In order to determine the dominating earthquake-related factors to the estimated CAV, all the combined data in the previous section for the attenuation model is now decomposed, a process known as disaggregation (or deaggregation). Through disaggregation process, the contribution of each earthquake to the considered ground motion (in this case CAV) can be known.

Fig. 7 shows the disaggregation for the CAV of 1.0, 3.5 and 8.9 m/s (a return period of 10, 160 and 2560 years, respectively). The notations M_m and R_m in the figure imply that the most dominant values of magnitude and distance (obtained as mean values), respectively, which contribute to the corresponding CAV. As can be seen, the concerned event at R = 10 years is dominated by earthquakes with relatively small magnitudes, while at R = 2560 years is controlled by earthquakes with high magnitudes. It appears that the distance to the source does not change with different return periods and the value is around 30 km. Together with the previous results shown in Fig. 6, it can be said that, at the Avara, there is 46 % chance that CAV

Table 1: Parameters of seismogenic zones

Zone name	α	β	M_{min}	M_{max}
W. Shiarnb	0.1546	2.21	4	6.0
Med1	0.3956	2.21	4	6.5
Beit Shean	0.0599	2.21	4	6.5
Jordan North	0.1044	2.21	4	5.5
Galil	0.0348	2.21	4	5.5
Roum	0.2887	2.21	4	7.5
Yamune	0.9144	2.21	4	7.75
Jordan V.	0.3729	2.21	4	7.5
Hula-Kineret	0.2526	2.21	4	7.5
Carmel	0.1199	2.21	4	6.5
Dead sea	0.2887	2.21	4	7.5
Central Israel	0.0232	2.21	4	5.5
Med2	0.2277	2.21	4	6.5
Med3	0.2158	2.21	4	6.5
Arava	0.3007	2.21	4	7.5
Suez	2.0425	2.46	4	7.0
Elat	0.1925	2.21	4	7.5
Aragonese	0.1925	2.21	4	7.5
Arnona	0.1925	2.21	4	7.5
Paran	0.0238	2.21	4	6.0
Barak	0.0371	2.21	4	5.5
Thamad	0.0642	2.21	4	6.0
Milhan	0.0162	2.21	4	5.5
Arif	0.0302	2.21	4	5.5
East Sinai	0.0333	2.21	4	6.0
Cyprus	2.7769	2.25	4	8.0
Palmira	0.1189	2.21	4	6.0

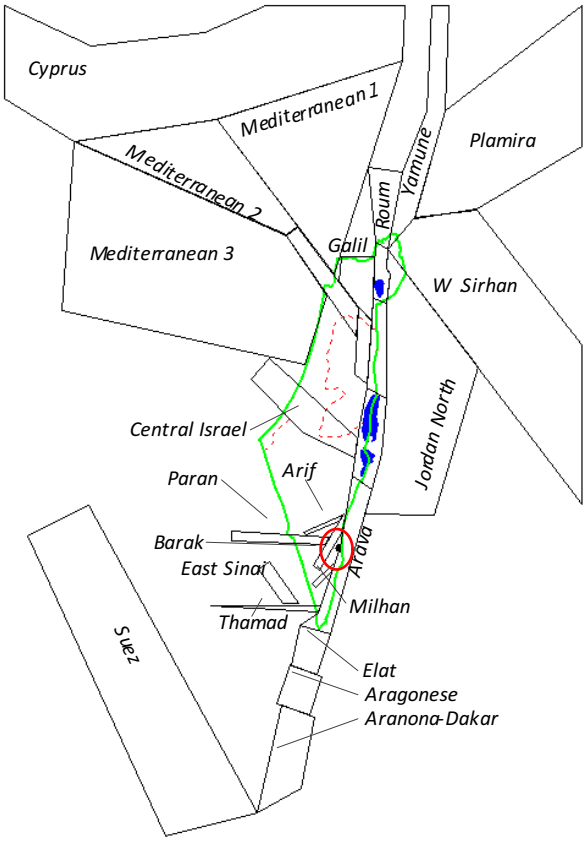

Figure 5: Seismogenic zones in Israel and adjacent areas

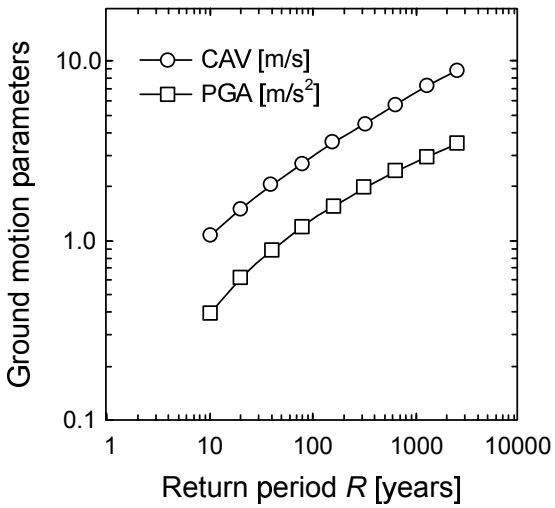

Figure 6: Expected CAV and PGA at a given return period for class D site

caused by earthquakes is likely to be 3.5 m/s (or greater) within 100 years and most likely will originate from earthquake distant by some 30 km.

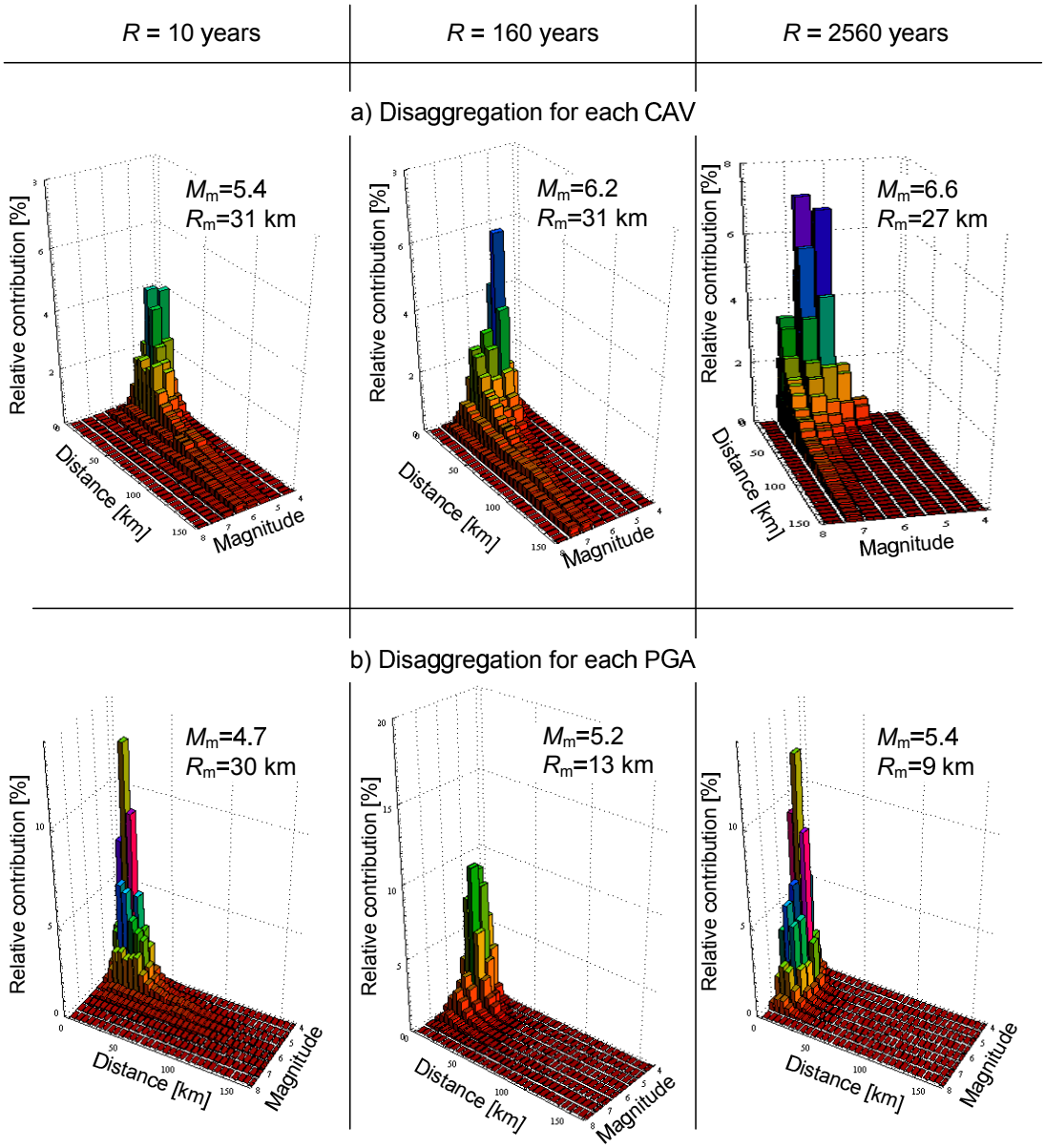

Figure 7: Disaggregation for the CAV and PGA

3.3 Selections of acceleration time history records

Considering the previous findings of most dominating magnitude and distance of earthquakes for a given CAV, a dataset of real earthquakes is constructed for time-domain analyses. Fig. 8 shows the acceleration time histories of selected earthquakes in this report. The information of the earthquake (e.g. event name, magnitude) is also shown in Fig. 8.

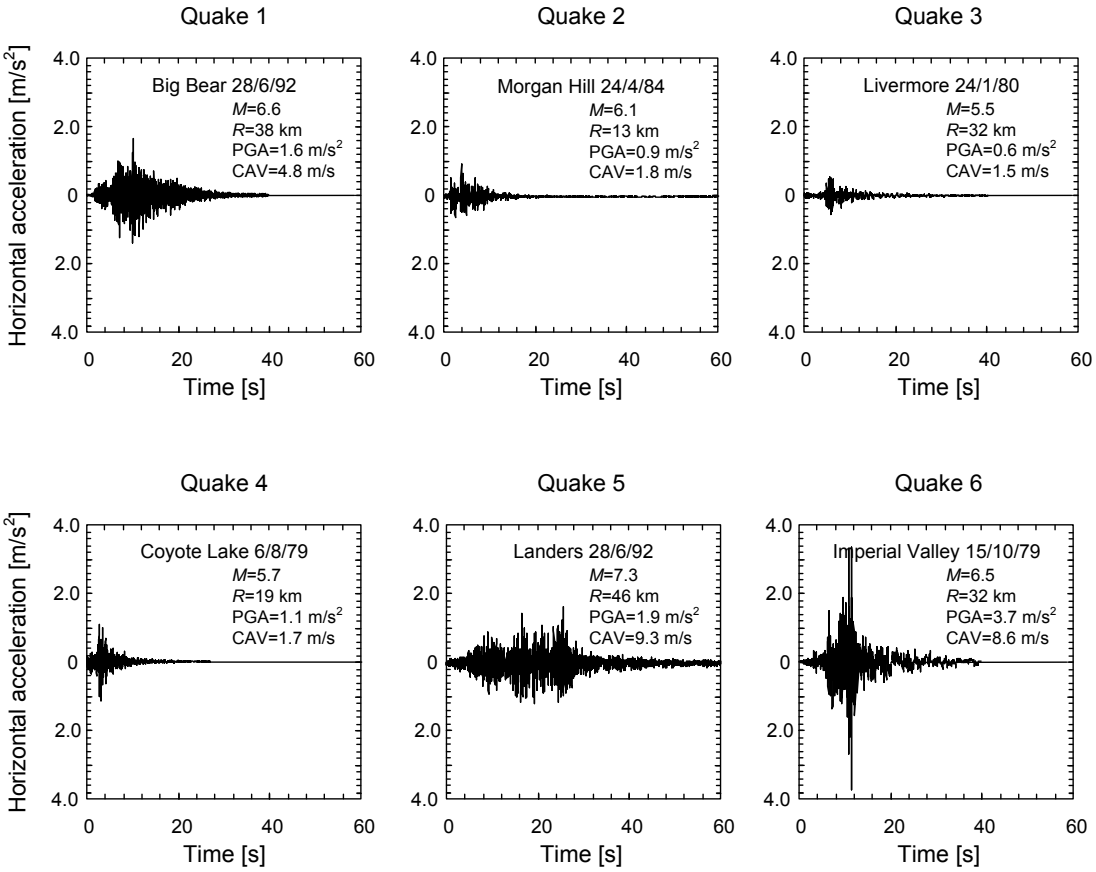

Figure 8: Selected earthquakes and their acceleration histories

Although it would be ideal that the selected earthquake induces the target CAVs, it is not often the case (it is, in fact, impossible to find an exact fit of characteristics). Thus, the selected earthquake is scaled (vertically) in order to shift the real CAVs into the target CAVs. By scaling the real CAV, the peak ground accelerations (PGA) of the earthquake is also scaled. While this paper does not study in detail the effect of PGA, the selected earthquakes are the ones that their scaled PGAs are also within the range of the target PGA. Table 2 lists the selected earthquakes, target CAV (which are also shown in Fig. 6) and corresponding scaled outcrop PGA.

It should be noted that the values of CAV and PGA shown in Table 2 are not exactly the same as the ones produced at the surface of the geomechanical analyses shown later, due to site effect regulations by the solution. This is because the soil is neither elastic nor homogeneous in the current work. In other words, if the soil was elastic, the exact input motion at the bedrock for the target surface CAVs could have been determined by deconvolution based on linear wave equations. Therefore, the analyses are conducted iteratively in order for the computed CAV values, in the free field surface, to fall within the considered range. It is found that the scaling for all conditions fall in the range of factors between 1/3 and 1.5.

Table 2: Parameters of seismogenic zones

Return Period R [years]		10	20	40	80	160	320	640	1280	2560
Target CAV [m/s]		1.04	1.47	2.00	2.65	3.45	4.44	5.63	7.06	8.72
Scaled outcrop PGA_{sc} [m/s^2]	Quake 1					1.20	1.55	1.97	2.47	3.05
	Quake 2	0.55	0.77	1.04	1.39	1.80				
	Quake 3	0.45	0.61	0.83	1.10	1.43				
	Quake 4	0.73	1.02	1.39	1.84					
	Quake 5						1.02	1.30	1.63	2.02
	Quake 6						1.93	2.46	3.08	3.80
Mean PGA_{sc} [m/s^2]		0.57	0.80	1.09	1.44	1.48	1.51	1.91	2.40	2.96
Target PGA [m/s^2]		0.39	0.60	0.87	1.18	1.53	1.94	2.38	2.87	3.39

As summarized in Table 2, for each return period, three different scaled earthquakes are applied to conduct geomechanical analyses. For example, for R = 10 years, Quake 2, Quake 3 and Quake 4 (all scaled to have CAVs to be approximately 1.04 m/s) are applied.

4 DEFORMATION PROFILES DUE TO EARTHQUAKES

Serviceability of the railway track would drop according to deformation of the embankment. Deflection of the embankment would also hinder serviceability. Thus, in this paper, the differential displacements (Δu_x, Δu_y, and Δu_z) are investigated (and later used for fragility curve). Displacements presented in this paper are obtained at the surface of the embankment. The analyses are conducted using a commercial finite difference programme $FLAC^{3D}$ [13] with dynamic option. The plastic soil models (cf. Fig. 3) and the spatially distributed and auto-correlated soil properties (cf. Fig. 4) are incorporated through Itasca's internal programming language.

4.1 Demonstration for CAV of 3.45 m/s (Return period of 160 years)

As the input acceleration histories are different in each direction, sediments and embankment are exposed to truly three-dimensional shaking movement, resulting in a complex behavior. Fig. 9 shows the displacement profile of embankment surface relative to the averaged surface displacement at the end of Quake 1 in the case of CAV $\approx$ 3.45 m/s for Soil 1, Soil 2 and Soil 3. The relative displacements are permanently induced due to cyclic loading and this contours can be an indicative of differential displacements. Due to the heterogeneity of soil properties, the displacements differ among Soil 1, Soil 2 and Soil 3 and even in the same soil they are not uniform. This induces a large relative displacement, which plays a key role for railway serviceability (discussed later). Since periodic boundaries are constructed for the model, the front and rear sides of the embankment produce the same displacements.

Fig. 10 shows the displacement profile relative to the averaged value under Quake 1, Quake 2 and Quake 3 within Soil 1 for CAV 3.45 m/s. Although all the quakes are scaled to have the same CAV and the heterogeneous soil properties are identical, each earthquake induces the embankment surface to behave differently from one to the others. Overall trends imply that the edge of the embankment slides downwards and the embankment surface settles relative to the ground surface.

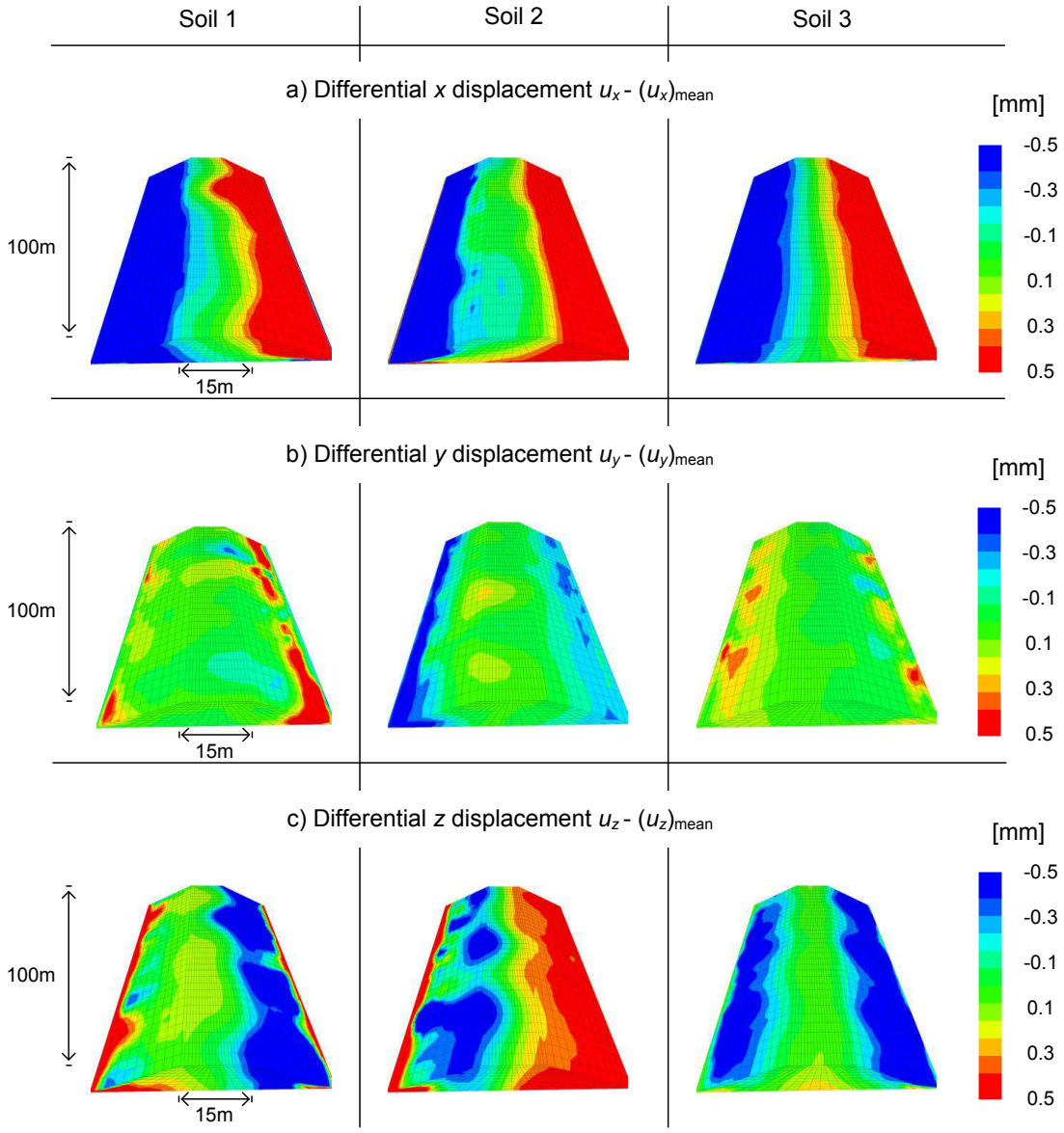

Figure 9: Displacement contours after Quake 1 for 3 soil patterns (CAV ≈ 3.45 m/s)

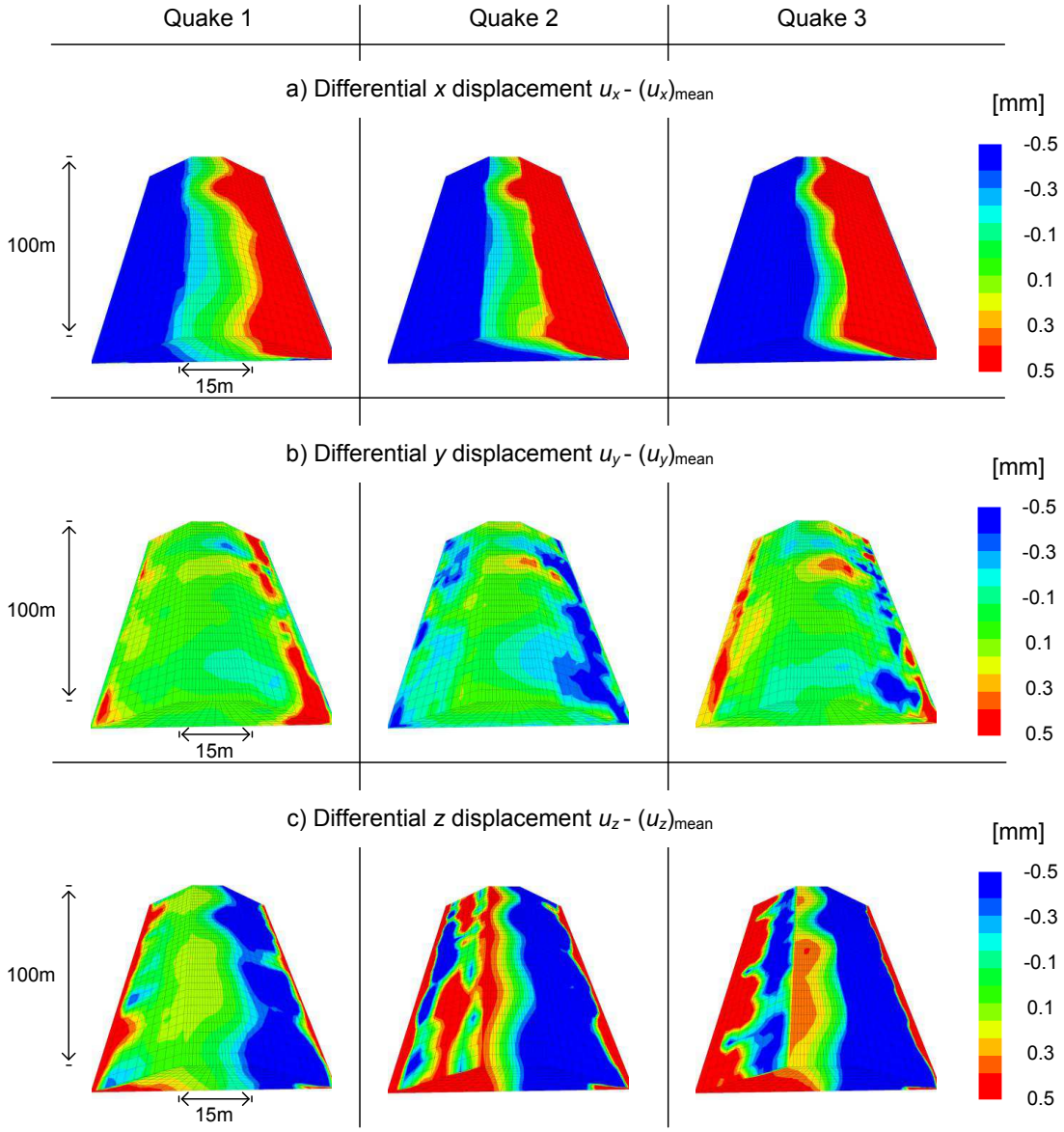

Figure 10: Displacement contours after 3 different earthquakes for Soil 1 (CAV ≈ 3.45 m/s)

4.2 CAVs of 1-10 m/s (Return periods of 10-3000 years)

The same analyses as the previous section are conducted for other 8 target CAVs, and in total 81 cases are considered (3 soil patterns times 3 earthquakes for 9 target CAVs). Fig. 11 presents the maximum differential permanent displacements with different CAVs. The maximum differential displacement is the maximum value of the induced relative displacements on the entire embankment surface. It is obvious that the displacements become larger when CAVs are larger. It may also be evident that at certain CAV levels the scatter becomes larger and the slope of the trend line changes. This trend relates to the onset of significant yielding of the embankment itself.

From the scattered data, deterministic relations of each differential displacement are obtained, which are also stated in Fig. 11 (denoted as the lines) with the standard deviation of each case (in natural logarithmic scale) is $s_{(\Delta u_x)_{max}}$=1.109, $s_{(\Delta u_y)_{max}}$=1.361 and $s_{(\Delta u_z)_{max}}$=1.049. As a result, the most likely induced permanent differential displacement of the embankment can be evaluated at a given CAV. For example, the maximum differential x displacement is approximately 15 mm when CAV = 5.6 m/s. This value is found in the same range of the estimated slope displacements by pseudostatistic analyses by [14] and [15] using corresponding PGA values found in Table 2. This finding supports the validity of the current analyses.

5 RAILWAY SERVICEABILITY CURVE

High-speed railway tracks require quality maintenance for track alignment retention, hence for safe train operation. High-speed railway tracks are especially vulnerable to differential deformations and evaluating deflections is a key engineering tasks associated with the train design. Table 3 lists examples of the serviceability standards for deflections of high-speed railway track.

Table 3: In service values for maximum railway deflections

Paulo Fonseca	German Regulation	IV International Congress	French Regulations
2.0 mm	1.5 mm	1.5 mm	1.5 mm

One may use the relation presented in the previous section (cf. Fig. 11) to evaluate the expected level of deformation using CAV in a deterministic manner. However, such evaluation would include significant uncertainty due to the scatter of the results. The framework of Probabilistic Seismic Hazard Analysis provides a consistent treatment of the problem by including the uncertainty implicitly in the calculation (and hence avoids the uncertainty). As a result, it enables to statistically evaluate the serviceability level of the railway track at the Arava.

A PSHA based formulations for such calculation can be written analytically as follows:

$$\lambda_{D^*} = \sum_{i=1}^{NS} \alpha_i \int\int\int P[D^*|CAV] \cdot f[CAV|m,r] \cdot f_{Mi}(m) \cdot f_{Ri}(r) dCAV\, dm dr \tag{12}$$

Or numerically as:

$$\lambda_{D^*} = \sum_{i=1}^{NS} \alpha_i \sum_{k=NXS_i}^{NXE_i} \sum_{l=NYS_i}^{NYE_i} \sum_{j=1}^{NMW} \int_{-\infty}^{\infty} P[D^*|\tau] \cdot f_{CAV}[m_j, r_{i,k,l}] d\tau f_{Mi,j} A_{i,k,l} \Delta m_i \tag{13}$$

$$P[D^*|CAV] = \frac{1}{\sqrt{2\pi}} \int_{\frac{\ln D^* - \ln D(CAV)}{s}}^{\infty} \exp[-\theta^2/2] d\theta \tag{14}$$

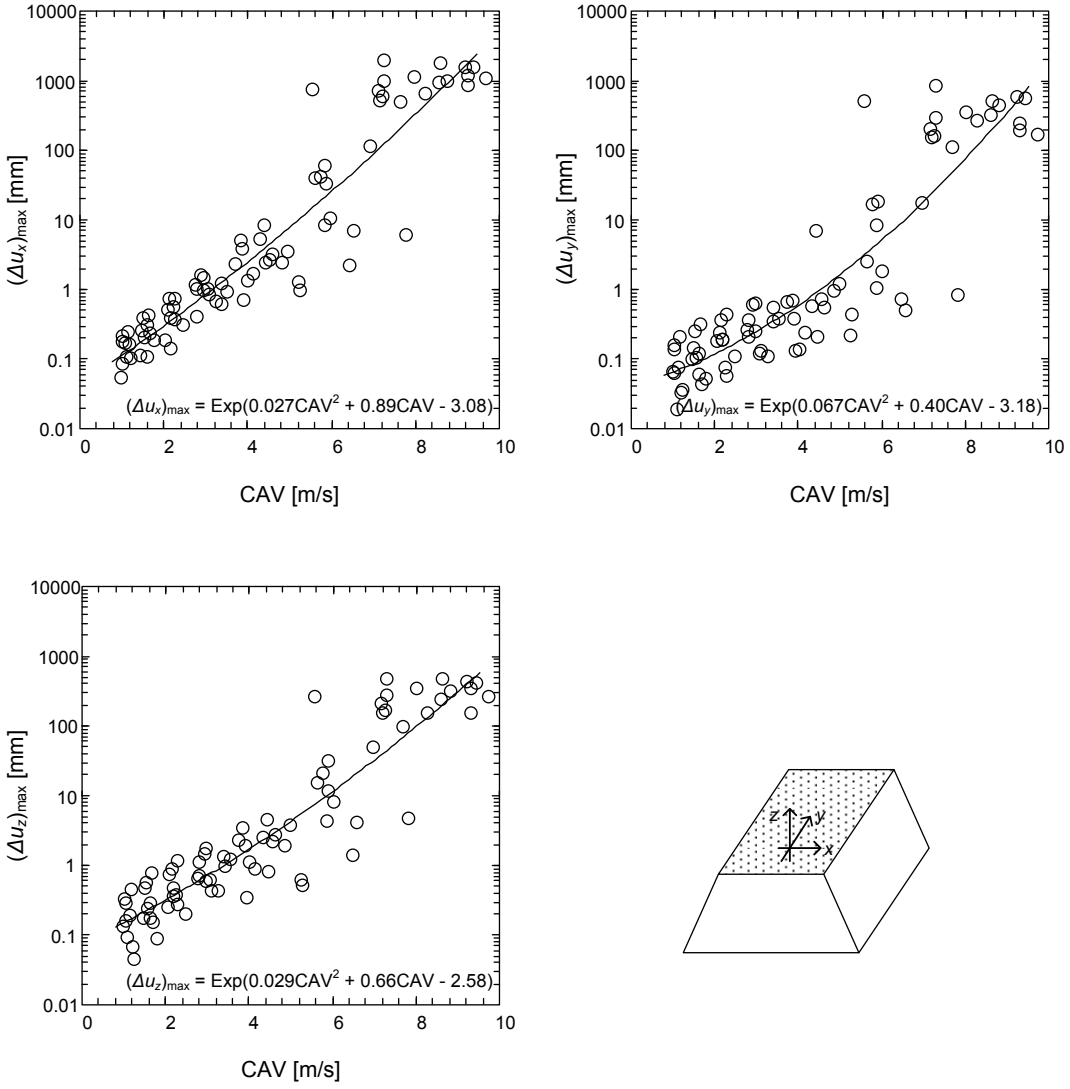

Figure 11: Maximum differential displacements with different CAVs (81 cases in total)

$$f_{CAV}[m_j, r_{i,k,l}] = \frac{1}{\sqrt{2\pi}} \exp\left[-\left(\frac{\tau - \ln CAV(m_j, r_{i,k,l})}{\sigma_{\ln CAV}}\right)^2 / 2\right] \quad (15)$$

where $\sigma_{\ln CAV}$ is the standard deviation of CAV as defined by [12] and s is the standard deviation of the natural logarithmic of the suggested curves for maximum differential displacements as given in the previous section. Essentially, the above equation is one order higher integration form of the conventional PSHA integral. Solving Eq. 13 results in the exceedance probability of D^* by a single event for a given exposure period t. In this work, it provides the answer to what the chance is in which a maximum differential displacement caused by a single earthquake would exceed the value D^* for a period of t.

Fig. 12 shows the solutions of Eq. 13 in each maximum differential displacement for exposure periods of 20, 40, 60, 80 and 100 years. The x axis is the maximum differential displacement and y axis is the exceedance probability. Thus, by drawing a straight vertical line to x axis, the intersection point to the curve represents its exceedance probability. For example, in the case of $(\Delta u_x)_{max}$, there is 8 % of chance that the differential displacement caused by a single earthquake would be greater than 2 mm within 20 years. The same line also states that the probability of exceeding the 2 mm value by a single earthquake event is 15 %, 21 %, 27 % and 33 % within periods of 40, 60, 80 and 100 years, respectively. Table 4 summarises the exceedance probability of the maximum differential displacement can be greater than 2 mm by a single event at Arava site.

Table 4: Exceedance probability of $(\Delta u)_{max}$ to be greater than 2 mm within exposure periods t

Exposure period t [years]	20	40	60	80	100
P[$(\Delta u_x)_{max} > 2$mm]	7.6 %	14.6 %	21.1 %	27.1 %	32.7 %
P[$(\Delta u_y)_{max} > 2$mm]	8.2 %	15.7 %	22.7 %	29.0 %	34.9 %
P[$(\Delta u_z)_{max} > 2$mm]	8.4 %	16.0 %	23.1 %	29.5 %	35.4 %

While an expected displacement induced by a single event has a great importance, it is also imperative to evaluate a cumulative displacement. For example, using Fig. 12, within 20 years of life cycle there is 88 % chance of the maximum differential x displacement to be greater than 0.25 mm, 51 % of greater than 0.5 mm and so on. Based on the Poisson's model (cf. Eq. 11), it is equivalent to the fact that, within 20 years, the event of 0.25 mm (or greater) deformation occurs on average 2.09 times, 0.5 mm deformation occurs on average 0.71 times and so on. If no regular alignment of railway is conducted, all these displacements may accumulate and eventually damage the railway to reach unserviceable state. Hence, by counting all possible events through statistical integration, the average rate of cumulative displacements are evaluated, which are: $(\Delta u_x)_{max}$ = 0.14 mm/year, $(\Delta u_y)_{max}$ = 0.13 mm/year and $(\Delta u_z)_{max}$ = 0.19 mm/year.

These annual values are, however, based on all the displacement values from return period of up to 4000 years and implicitly take account of extreme rare events. This implies that even though the event hardly occurs within the considered exposure period t (e.g. for R=4000 year event, 99.75 % chance of zero occurrence, 0.25 % chance of once, 0.0003 % chance of twice and so on within 100 years), the statistical integration still counts the value. In order to avoid this, the cumulative displacement is recalculated based on all possible combinations of events that comprise 95 % cumulative probability of occurring within the considered return period t (conducting the recalculation with 100 % leads to the same average value as stated above). This approach, in effect, drops out rare events within the considered exposure period t and thus the

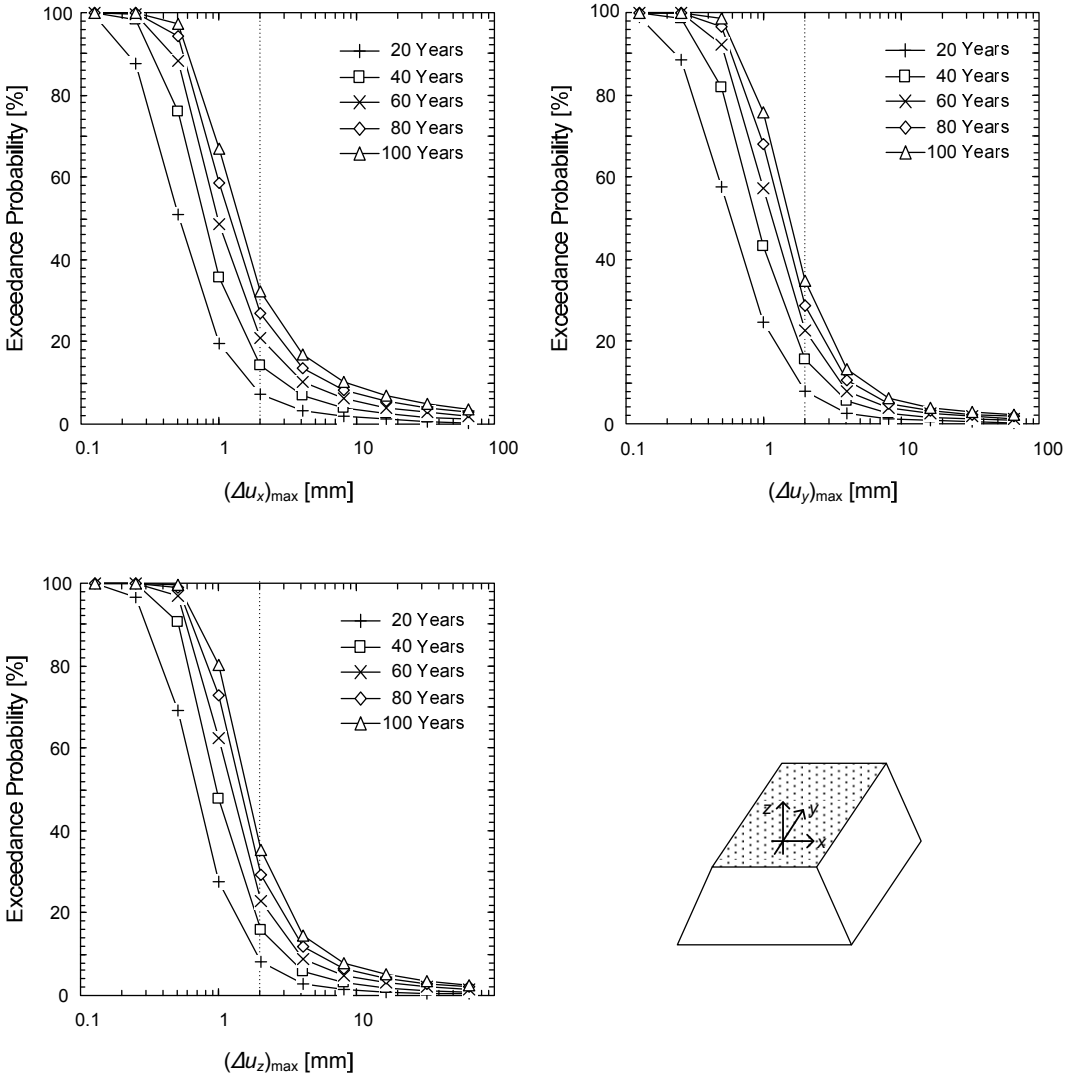

Figure 12: Exceedance probability of a maximum differential displacement

average rate becomes dependent on the considered exposure period. Assuming the exposure period of 100 years (i.e. a design life of the railway track is 100 years), the resulting values are summarised in Table. 5. It states that the limit of 2 mm deflection may be reached every 15 years, on average, throughout a life time of 100 years.

Table 5: Cumulative differential displacement for a design life of 100 years

	Annual rate	To reach 2 mm
$\Sigma(\Delta u_x)_{max}$	0.084 mm/year	23.9 years
$\Sigma(\Delta u_y)_{max}$	0.085 mm/year	23.5 years
$\Sigma(\Delta u_z)_{max}$	0.131 mm/year	15.3 years

6 CONCLUSIONS

This document presented a statistical analysis for the expected seismic induced differential deformation along the surface of the railway tracks of the Be'er-Sheval Eilat Train. The methodology was rather complex and involved integration of all possible earthquake events, together with nonlinear soil behaviour evaluation through advanced numerical and statistical analysis. It also included consideration of soil heterogeneity without which differential deformation would not be obtained from any numerical analysis.

The results presented in this document are relevant to a 10 metre heigh embankment over a natural soil Class-D site located in the middle section of the train route at the Arava. For the considered case, the statistical analysis indicated that there is a 35 % probability that the serviceability limit deflection value of 2 mm may be reached by a single event within the lifespan of 100 years. By considering the cumulative deformation for multiple events, it is estimated that this limit would be reached every 15 years, on average, in the next 100 years.

7 Acknowledgment

The presented analysis in the paper was conducted as part of seismic consulting for Netivey Israel - The Israeli National Round and Infrastructure Company. We wish to thank the engineers involved in the project for the discussion on the different issues of the problem. In specific, Eng. Dan Gronner of Gronner D.E.L. and Enggineers and Eng. Eliezer Shamir and Ronen Brown of Shamir-Posner-Brown Cons. Engineers LTD.

REFERENCES

[1] R. McGuire, Probabilistic seismic hazard analysis and design earthquakes: closing the loop, Bulletin of the Seismological Society of America 85 (5) (1995) 1275–1284.

[2] H. Seed, I. Idriss, Simplified procedure for evaluating soil liquefaction potential, Journal of Soil Mechanics & Foundations 97 (9) (1971) 1249–1273.

[3] P. Byrne, A cyclic shear-volume coupling and pore-pressure model for sand, in: Second International Conference on Recent Advances in Geotechnical Earthquake Engineering and Soil Dynamics, Missouri, 1991, pp. 47–55.

[4] M. E. Harr, Reliability-based Design in Civil Engineering, McGraw-Hill Inc., New York, 1987.

[5] H. El-Ramly, N. Morgenstern, D. Cruden, Probabilistic slope stability analysis for practice, Canadian Geotechnical Journal 39 (3) (2002) 665–683.

[6] H. B. Seed, R. T. Wong, I. M. Idriss, K. Tokimatsu, Moduli and Damping Factors for Dynamic Analyses of Cohesionless Soils, Journal of Geotechnical Engineering 112 (11) (1986) 1016–1032.

[7] M. Kostov, Site specific estimation of Cumulative Absolute Velocity, in: 18th International Conference on Structural Mechanics in Reactor Technology, Beijing, China, 2005, pp. 3041–3050.

[8] J. Klugel, L. Mualchin, G. Panza, A scenario-based procedure for seismic risk analysis, Engineering Geology 88 (2006) 1–22.

[9] S. Kramer, R. A. Mitchell, Ground motion intensity measures for liquefaction hazard evaluation, Earthquake Spectra 22 (2006) 413–438.

[10] L. Danciu, G.-A. Tselentis, Engineering Ground-Motion Parameters Attenuation Relationships for Greece, Bulletin of the Seismological Society of America 97 (1B) (2007) 162–183.

[11] G. Shamir, Y. Bartov, A. Sneh, L. Fleischer, V. Arad, M. Rosensaft, Preliminary seismic zonation in israel, Technical Report 550/95/01, Geophysical Institute of Israel (2001).

[12] K. Campbell, Y. Bozorgnia, A ground motion prediction equation for the horizontal component of cumulative absolute velocity (CAV) based on the PEER-NGA strong motion database, Earthquake Spectra 26 (3) (2010) 635–650.

[13] Itasca, FLAC3D 4.0 - User's Guide, Itasca Consulting Group Inc., Minneapolis, USA, 2009.

[14] N. N. Ambraseys, J. M. Menu, Earthquake-induced ground displacements, Earthquake Engineering & Structural Dynamics 16 (7) (1988) 985–1006.

[15] J. Bray, T. Travasarou, Simplified procedure for estimating earthquake-induced deviatoric slope displacements, Journal of Geotechnical and Geoenvironmental Engineering 133 (4) (2007) 381–392.